Title	Mono-sized single-wall carbon nanotubes formed in channels of AlPO4-5 single crystal
Author(s)	Tang, Z. K.; Sun, Handong; Wang, J.; Chen, J.; Li, G.
Citation	Tang, Z. K., Sun, H. D., Wang, J., Chen, J., & Li, G. (1998). Mono-sized single-wall carbon nanotubes formed in channels of AlPO4-5 single crystal. Applied Physics Letters, 73(16), 2287-2289.
Date	1998
URL	http://hdl.handle.net/10220/6156
Rights	Applied Physics Letters © copyright 1998 American Institute of Physics. The journal's website is located at http://apl.aip.org/.

Mono-sized single-wall carbon nanotubes formed in channels of $AlPO_4$-5 single crystal

Z. K. Tang,[a] H. D. Sun, and J. Wang
Physics Department, Hong Kong University of Science and Technology, Clear Water Bay, Kowloon, Hong Kong, People's Republic of China

J. Chen and G. Li
Department of Chemistry, Jilin University, Changchun 130023, People's Republic of China

(Received 8 June 1998; accepted for publication 13 August 1998)

An alternative approach to the synthesis of *mono-sized* and parallel-aligned single-wall carbon nanotubes (SWCNs) is reported. The SWCNs are formed in 0.73 nm sized channels of microporous aluminophosphate crystallites by pyrolysis of tripropylamine molecules in the channels. They are characterized through transmission electron microscopy, polarized Raman scattering, and electrical transport measurements. Our results would open a door to further detailed studies on the intrinsic properties of carbon nanotubes now in progress. © *1998 American Institute of Physics.* [S0003-6951(98)00442-2]

Carbon nanotubes, originally discovered as a byproduct of fullerene research,[1] are attracting increasing interest as they offer new prospects to fundamental as well as nanotechnological applications.[2] An important recent advance in carbon nanotube science is the synthesis of single-wall carbon nanotubes (SWCNs) in high yield using the laser ablation method[3] and the electric arc technique.[4] In each case, a small amount of transition metal was added to the carbon target as a catalyst. However, it is still a big challenge to produce *mono-sized* SWCNs with well-defined symmetry, and to make a good electrical contact to a single nanotube for carrying out experimental investigations. Here we report an alternative approach to the synthesis of *mono-sized* and parallel-aligned SWCNs in channels of microporous single crystal by pyrolysis of tripropylamine (TPA). The nanotube structure is confirmed using the transmission electron microscopy (TEM) observation. The SWCNs are characterized by polarized Raman scattering and electrical transport measurements. The fabrication of monodispersed SWCNs in three-dimensional ordered and nano-sized channels represents an important step towards the development and applications of carbon nanotube materials.

Microporous aluminophosphate $AlPO_4$-5 crystals (AFI) with elongated hexagonal prisms of dimensions 110 μm in cross-section diameter and 300 μm in length were used as the hosts to encapsulate the SWCNs. The framework of the AFI crystal is constructed of alternative tetrahedra of $(AlO_4)^-$ and $(PO_4)^+$, which form parallel open channels packed in the hexagonal structure. The coordinate diameter of the channels is 10.1 Å (inner diameter 7.3 Å), and the separation distance between two neighboring channels is 13.7 Å. The AFI host was synthesized according to the method given in Ref. 5. TPA molecules were encapsulated in the channels during the crystal growth. The synthesis procedure of the SWCNs involves the pyrolysis of TPA molecules in the AFI channels in a vacuum of 10^{-4} Torr at temperatures of 350–450 °C and the formation of carbon nanotubes at 500–800 °C. The formation of the SWCNs is very sensitive to the quality of the AFI crystal, the encapsulation of hydrocarbon molecules in the AFI channels, and the pyrolysis conditions. The carbon nanotube contained AFI crystal (C-AFI) behaves as a good polarizer with high absorption for the light polarized parallel to the channel direction ($E \| c$) and with a high transparency for $E \perp c$, consisting of the one-dimensional characteristics of the nanotubes.

Figure 1 shows the TEM image of the nanotubes exposed in free space after removing the AFI framework using HCl acid. The image was taken using a Philips CM200 at 200 keV. Smoothly bent wire-like carbon specimens, with a separation distance of about 7 Å, are seen in the image. We attribute the wire-like carbon specimen to SWCNs. The diameter of the SWCNs is expected to be smaller than 7 Å. The structure of the small SWCNs is stable when they are confined in the channels of AFI crystal, but they are unstable

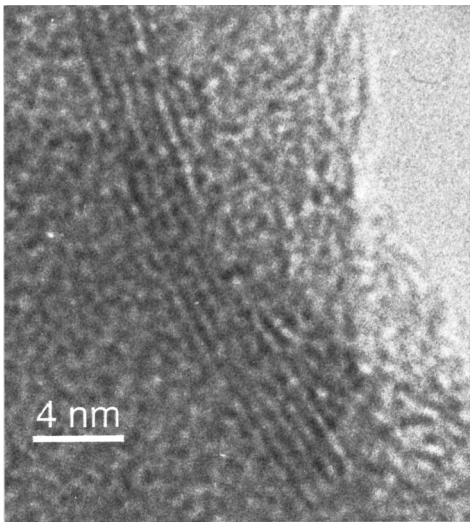

FIG. 1. Transmission electron microscope (TEM) image shows the SWCNs which are slightly bent. The TEM image was taken after the AFI framework was removed using HCl acid, and the SWCNs were exposed in free space.

[a]Electronic mail: PHZKTANG@usthk.ust.hk

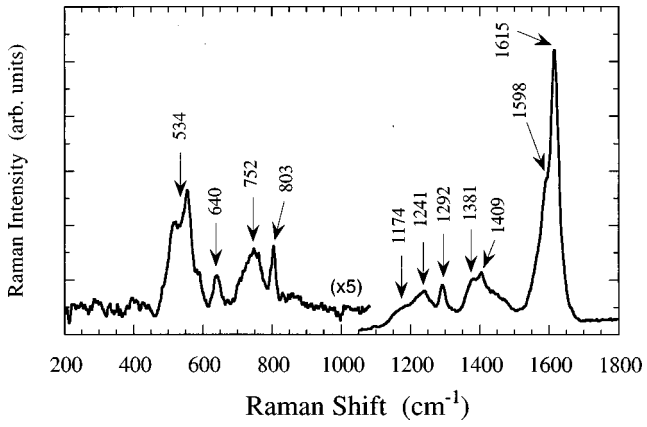

FIG. 2. Raman spectrum of the SWCNs measured at room temperature using the 632.8 nm line of a He–Ne laser as the excitation.

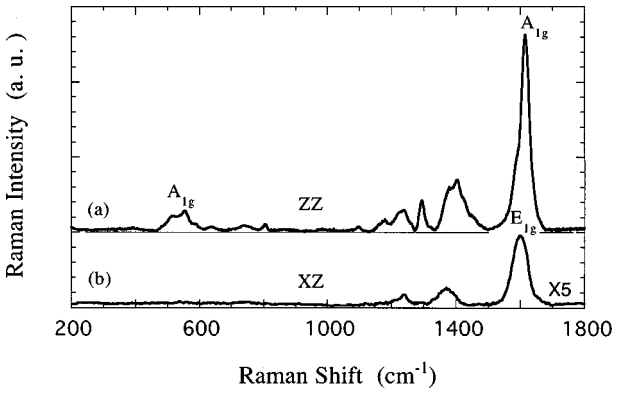

FIG. 3. Polarized Raman spectra of the SWCNs measured in (a) *ZZ* configurations, and (b) *XZ* configuration. In the *ZZ* configuration, the polarizations of the incident and the scattered lights are parallel to each other and are polarized along the nanotube direction; in the *XZ* configuration the polarizations of the incident and the scattered lights are perpendicular to each other.

when they are exposed into free space especially under electron-beam irradiation. This fact indicates that the one-dimensional channels of AFI crystal plays an important role in stabilizing small carbon nanotubes.

It is difficult to determine the configuration of the SWCNs accurately from electron microscopy, but the nanotube configuration can be studied in detail using Raman spectroscopy. Figure 2 shows Raman spectra of the SWCNs using a 632.8 nm line of a He–Ne laser as excitation. The Raman spectrum exhibits three main zones at low ($200-800\ \mathrm{cm}^{-1}$), intermediate ($1000-1500\ \mathrm{cm}^{-1}$), and high ($1500-1620\ \mathrm{cm}^{-1}$) frequencies. The strongest low-frequency Raman mode at $534\ \mathrm{cm}^{-1}$ is expected to be the radial breathing A_{1g} mode. This frequency is in the silent region for graphite and the other carbon materials. Hence, it is a good marker for specifying the carbon nanotube structure. The radial breathing A_{1g} mode is not sensitive to nanotube structure but to the nanotube radius. The observed frequency of $534\ \mathrm{cm}^{-1}$ is, however, a little higher than that expected for a nanotube with a radius of about 3 Å.[6] This high-frequency shift may result from the interaction between the nanotube wall and the rigid wall of the AFI channel. In the high-frequency zone, there is a main Raman band at $1615\ \mathrm{cm}^{-1}$ with a shoulder at $1598\ \mathrm{cm}^{-1}$. According to the calculation,[6,7] some modes with symmetries of A_{1g}, E_{1g}, and E_{2g} are expected in this frequency region. These Raman modes are sensitive to polarization configuration. Thus, measurement of polarized Raman scattering can specify the different vibration modes. Figure 3 shows the polarized Raman spectra. Curve (a) is measured in a *ZZ* configuration in which the incident and the scattered polarizations are parallel to each other along the tube direction, while curve (b) is measured in a *XZ* configuration in which the incident and the scattered polarizations are perpendicular to each other. The intensity of the Raman signal in the *ZZ* configuration is much stronger than those in all other polarization configurations, indicating the one-dimensional characteristics of the carbon specimen accommodated in the AFI channels. As seen in Fig. 3, the Raman spectrum in the *ZZ* configuration is dominated by the $534\ \mathrm{cm}^{-1}$ band in the low-frequency zone and the $1615\ \mathrm{cm}^{-1}$ band in the high-frequency zone. These two bands are absent in the *XZ* configuration. Instead, the spectrum in the *XZ* configuration is dominated by the $1598\ \mathrm{cm}^{-1}$ band. According to the symmetry and the polarization selection rules for a zigzag $(n,0)$ or an armchair (n,m) nanotube,[6] the A_{1g} mode is allowed but the E_{1g} and E_{2g} modes are forbidden in the *ZZ* configuration. The E_{1g} is allowed and the A_{1g} and E_{2g} modes are forbidden in the *XZ* configuration. Comparing the polarization behavior of Raman spectra in Fig. 3 with the polarization selection rules, the bands at 534 and $1615\ \mathrm{cm}^{-1}$ can be assigned to A_{1g} modes, and the band at $1598\ \mathrm{cm}^{-1}$ to the E_{1g} mode. The presence of the E_{1g} as a shoulder in the *ZZ* configuration (curve a) might be due to a slight relaxation of the E_{1g} mode selection rule because of some possible structure defects in the SWCNs.

The electric transport properties are also studied for the SWCNs. In order to carry out electrical measurements, the sample was vertically fixed using epoxy inside a small hole drilled on a machinable ceramic. Both sides of the sample were then polished until the hexagon ends of the crystal were exposed. Electrical contacts were made by evaporating a thin layer of gold on both end surfaces, as shown in Fig. 4(a). Current–voltage ($I-V$) properties are measured in the temperature range from 0.3 to 300 K. The inset of Fig. 4(b) shows the conductivity σ of the SWCNs measured near zero voltage, plotted in logarithm scale as a function of the temperature T. At room temperature the conductivity of the SWCN is on the order of $10^{-1}\ \Omega^{-1}\ \mathrm{cm}^{-1}$, which is lower than the reported conductivity of metallic single-wall carbon nanotubes.[8–10] It is worthwhile to point out that the backbone of the AFI crystal with or without TPA in the channels is highly insulating. It contributes a current at least five orders of magnitude smaller than that of C-AFI samples. The conductivity of the SWCNs is monotonically increased with increasing temperatures, indicating that the SWCN is of semiconductor characteristics. The typical dc $I-V$ curve (open circles) measured at different temperatures is plotted in log–log scale in Fig. 4(b). The solid lines are fittings with $I \propto V$ and $I \propto V^{3/2}$ as indicated in Fig. 4. The current starts out as a linear function of the voltage, but switches to a $V^{3/2}$ behavior when the bias voltage is high or when the temperature is low. Since the SWCNs in our experiment are not intentionally doped, the conducting carriers are expected to be due to the thermally generated free carriers. Because the electrode

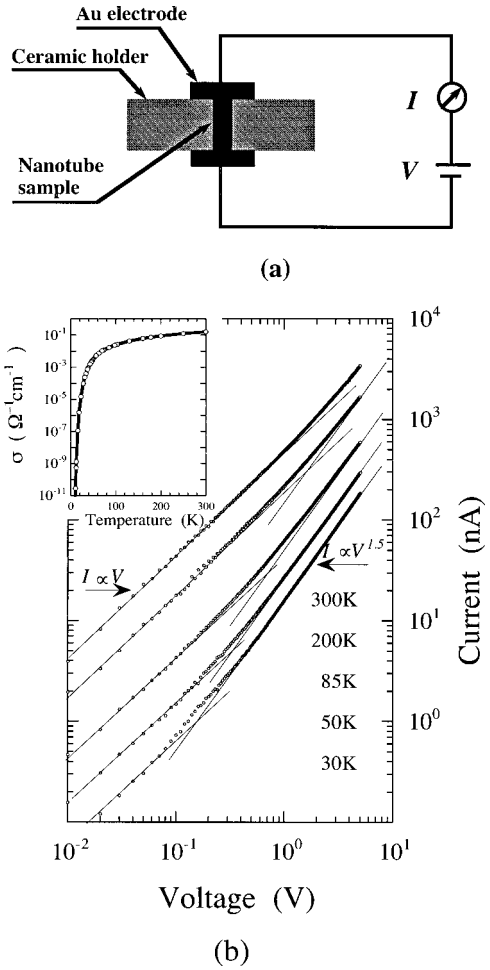

FIG. 4. (a) Schematic diagram illustrating the experimental setup for electrical measurements for the SWCNs, and (b) the experimental dc $I-V$ curves (open circles) at different temperatures plotted on a log–log scale. The fittings are shown as solid lines with $I \propto V$ in the low bias region and $I \propto V^{3/2}$ in the high bias region. The inset of (b) shows the conductivity measured near zero bias as a function of temperature.

metal and the SWCN have different work functions, a Schottky barrier can be formed at the lead–sample contact. When a bias is applied, the barrier prevents one type of the thermally excited carriers (say electrons) to pass through, but allows the other type of carriers (say holes) to pass through freely. Hence, electrical conduction in the SWCN is expected to be a *single-carrier* process. A quantitative description of the experimental $I-V$ curves can then be obtained by evaluating the current across the sample by using the transport equation[11,12]

$$J = q\mu(n+n_0)E \tag{1}$$

and the Poisson equation

$$\frac{1}{r}\frac{d(r^2E)}{dr} = \frac{qn}{\epsilon}, \tag{2}$$

where q is the carrier charge, μ is the carrier drift mobility, E is the applied electric field, ϵ is the static electric constant, and n and n_0 are the free carrier density injected from the electrode and the thermally generated carrier density, respectively. At high temperature or low bias voltage, $n_0 \gg n$, the current is simply given by Eq. (1): $I_\Omega = I_{\Omega 0}\mu(n+n_0)V$, which is bulk limited and is a linear function of bias voltage V (ohmic current). At low temperature or under high bias, n is comparable with n_0. Solving Eqs. (1) and (2) yields $I_{\mathrm{SCL}} = I_{S0}\mu n_0^{1/2}V^{3/2}$, which is the so-called space-charge-limited (SCL) current. At a given temperature, the total current of the sample is due to the superposition of the I_Ω and the I_{SCL}. We expect the current to be dominated by I_Ω at low bias and high temperature and by I_{SCL} at high bias and low temperature. The solid lines in Fig. 4(b) show the calculated currents at different temperatures. The good agreement between experimental data and calculation also indicates that the SWCN confined in the AFI channel is an intrinsic semiconductor.

In summary, we have fabricated *mono-sized* SWCNs with well-defined structure symmetry. They were characterized through TEM, Raman scattering, and electrical transport measurements. Our results would open a door to further detailed studies on the intrinsic properties of semiconducting carbon nanotubes presently underway.

The authors are grateful to Professor L. L. Chang, Professor M. M. T. Loy, Professor P. Sheng, and Professor G. K. L. Wong for their encouragement and valuable comments. In particular, H. D. Sun is grateful to Professor G. K. L. Wong for introducing him to this research area. The authors thank Dr. C. T. Chen for his theoretical advice and useful discussion. The TEM image was taken by Dr. N. Wang. This research was supported by the RGC Committee of Hong Kong, and the EHIA program from HKUST. J. Chen and G. Li would like to acknowledge the support from the National Natural Science Foundation of China.

[1] S. Iijima, Nature (London) **345**, 56 (1991).
[2] See, for example, a recent review book by M. S. Dresselhaus, G. Dresselhaus, and P. C. Eklund, *Science of Fullerenes and Carbon Nanotubes* (Academic, New York, 1996).
[3] T. Guo, P. Nikolaev, A. Thess, D. T. Colbert, and R. E. Smalley, Chem. Phys. Lett. **243**, 49 (1995).
[4] C. Journet, W. K. Maser, P. Bernier, A. Loiseau, M. Lamy de la Chapelle, S. Lefrant, P. Deniard, R. Lee, and J. E. Fischer, Nature (London) **388**, 756 (1997).
[5] S. Qiu and W. Pang, Zeolites **9**, 440 (1989).
[6] R. Saito, T. Takeya, T. Kimura, G. Dresselhaus, and M. S. Dresselhaus, Phys. Rev. B **57**, 4145 (1998).
[7] P. C. Eklund, J. M. Holden, and R. A. Jishi, Carbon **33**, 959 (1995).
[8] A. Thess, R. Lee, P. Nikolaev, H. Dai, P. Petit, J. Robert, C. Xu, Y. H. Lee, S. G. Kim, A. G. Rinzler, D. T. Colbert, G. E. Scuseria, D. Tombnek, J. E. Fischer, and R. E. Smalley, Science **273**, 483 (1996).
[9] T. W. Ebbesen, H. J. Lezec, H. Hiura, J. W. Bennet, H. F. Ghaemi, and T. Thio, Nature (London) **382**, 54 (1996).
[10] A. Yu Kasumov, I. I. Khodos, P. M. Ajayan, and C. Colliex, Europhys. Lett. **34**, 429 (1996).
[11] M. A. Lampert, A. Many, and P. Mark, Phys. Rev. **135**, A1444 (1964).
[12] K. C. Kao and W. Hwang, *Electrical Transport in Solids* (Pergamon, London, 1981).